

# Pose-Based Servo Control with Soft Tactile Sensing

Nathan F. Lepora\* and John Lloyd\*

**Abstract**—This paper describes a new way of controlling robots using soft tactile sensors: pose-based tactile servo (PBTS) control. The basic idea is to embed a tactile perception model for estimating the sensor pose within a servo control loop that is applied to local object features such as edges and surfaces. PBTS control is implemented with a soft curved optical tactile sensor (the BRL TacTip) using a convolutional neural network trained to be insensitive to shear. In consequence, robust and accurate controlled motion over various complex 3D objects is attained. First, we review tactile servoing and its relation to visual servoing, before formalising PBTS control. Then, we assess PBTS over a range of regular and irregular objects. Finally, we reflect on the relation to visual servo control and discuss how controlled soft touch gives a route towards human-like dexterity in robots.

## I. INTRODUCTION

THE human tactile sense enables us to use our hands to manipulate and explore our surroundings. The extent of our handiwork is a uniquely human capability that has, for better or worse, transformed the world around us: all of our technology stems ultimately from devices made by hand. An artificial tactile sense and the capability to explore and manipulate the surroundings will enable robots to perform manual tasks currently needing human labour. This has been the goal of tactile robotics research for half a century [1].

However, simple tactile tasks that are routinely performed by humans still elude robots, such as feeling around everyday objects. While there have been major advances in tactile sensors and their integration into robot hands [2], [3], their capabilities fall far short of human dexterity. In our view, a necessary yet underdeveloped ability is to control a soft tactile sensor to maintain contact while sliding over a surface. This is the robot analogue of tracing our fingertips over objects, called tactile servo control [4]–[9]. Without the ability to control how a soft fingertip interacts with an object, it is difficult to imagine how more complex tasks involving touch could be achieved.

Although there have been intermittent advances in tactile servo control, both the development of the field and the volume of research lag far behind visual servo control. The modern view of visual servoing emerged in the 1990s with two archetypal schemes: image-based and pose-based visual servo control [10]. However, almost all developments in tactile servo control have been based on image-based servoing [11] using image features from hard, planar tactile arrays [5]–[7], [9]. In this paper, we describe a framework based on the second

archetypal scheme, pose-based tactile servo control, and apply it to a soft tactile sensor.

The main contributions of this work are to:

- 1) Formalise *pose-based tactile servo* (PBTS) control, in which a model that relates tactile images to sensor poses is used to control the sensor pose directly.
- 2) Implement PBTS control with a soft tactile sensor and a model trained with deep learning to be insensitive to the sensor shear that occurs during soft interactions [12].
- 3) Test PBTS control by sliding over 3D surfaces and edges. Regular objects were used to measure performance and irregular objects to demonstrate generality.

This work builds on recent progress in learning a convolutional neural network model of sensor pose for the BRL TacTip [12], [13], a soft biomimetic optical tactile sensor [14], [15].

## II. BACKGROUND

### A. Tactile servo control

In control engineering, a *servomechanism* (shortened to ‘servo’) is an automatic device that uses error-sensing negative feedback to correct the action of a mechanism. The field of robotics relies on using servomotors (shortened to ‘servos’) that precisely control their motion and final position.

In modern robotics, *visual servo control* has received a huge amount of interest, and is based on using computer vision data in the servo loop to control the motion of a robot [10]. Research on visual servoing dates back four decades [16] with the modern view emerging in the 1990s [17]–[20]. A fundamental aspect of the formalism is that it distinguishes two archetypal schemes, known as *image-based visual servo* (IBVS) control and *pose-based visual servo* (PBVS) control, which differ in the type of feedback error used in the controller. The image-based scheme controls a feature vector extracted from the 2D image in the sensor frame of that image, whereas the pose-based scheme controls the camera pose directly in the Cartesian space (base frame) of the robot (Figure 1).

This distinction between image-based and pose-based control has helped the research field of robot vision progress, with pros and cons of the two schemes (and hybrid schemes) still being investigated. The image-based scheme benefits from using image features that can be extracted straightforwardly in the control loop (e.g. image moments or key points on the image). However, the controller outputs a change in feature vector, which must be transformed to a motion of the camera, and this inverse transformation can be challenging to compute, usually with an approximate ‘interaction matrix’ for a given scenario. The pose-based scheme benefits from controlling the

N. Lepora and J. Lloyd are with the Department of Engineering Mathematics, Faculty of Engineering, University of Bristol and Bristol Robotics Laboratory, Bristol, UK. e-mail {n.lepora, jl15313}@bristol.ac.uk.

\* NL and JL contributed equally to this work.

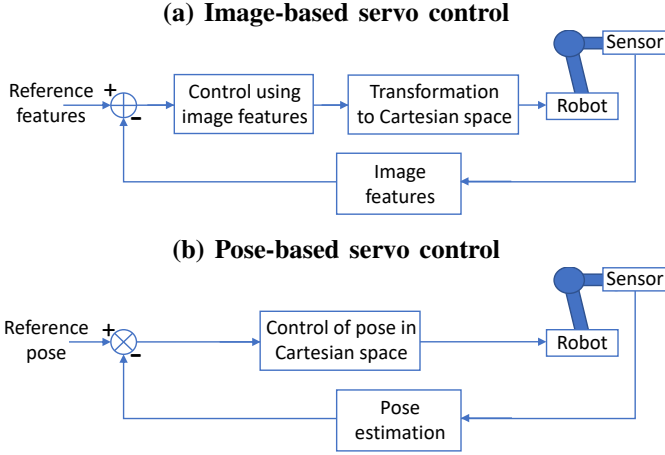


Figure 1. Two archetypal schemes for feedback control of sensorized robots: (a) image-based and (b) pose-based servo control (based on [19, Figs 5,6]). The schemes differ in how the sensor image is used in the controller: to generate image features or estimate pose, and thus whether the control is in Cartesian space (the base frame of the robot) or not.

camera position and orientation directly, but requires a 3D model of the object to estimate its pose from the camera image, which likewise can be difficult to calculate.

*Tactile servo control* has received far less attention and its fundamentals are still being developed. The first complete treatment on control of contact via tactile sensing was developed two decades ago by Zhang and Chen [6], building upon earlier work on tactile edge tracking [4], [5] and object manipulation [11], [21]. The control of contact relied on extracting tactile features as the input to a controller whose output fed through an ‘inverse tactile Jacobian’ that related these features in the image frame to the sensor motion in the Cartesian space (base frame) of the robot. Extraction of the tactile features relied on a finite element model of the sensor to infer the normal force and centre of contact from a tactile image. Evidently, this scheme is the tactile analogue of image-based visual servoing [9], [11]. Hence, we refer to it as *image-based tactile servo* (IBTS) control, where we interpret a *tactile image* as data from an array of tactile elements called *taxels* or *tactels*, which are akin to pixels of a visual image.

Tactile servo control had a hiatus for a decade before development continued on a control framework for tactile servoing [7], [22]. Li *et al* simplified Zhang and Chen’s treatment by using a hard planar tactile array from which relevant tactile features can be estimated and controlled directly: a 2D centre of contact, normal force and orientation (from the centroid, area and moments of the tactile image). The inverse Jacobian that relates the controller output to the sensor motion was approximated with a linear transformation, analogous to the interaction matrix in IBVS control. By setting this matrix, they demonstrated tactile servoing tasks from normal force control and tracking a horizontal contact to rolling around a cylinder and sliding along a horizontal cable [7]. Recently, Kappassov *et al* extended this control scheme to six features, by also including the centre of pressure, to control the sensor pose on more complex 3D tasks [9]. With an appropriate inverse Jacobian matrix, the range of tasks was extended to slide along a bent bar in 3D and to orient to balance a tray.

Around the same time, another scheme was developed for tactile contour-following around planar objects, using a curved, soft tactile sensor (an iCub fingertip) with a Bayesian predictor of 2D sensor pose [23], [24]. Although the sensor motion was not described in standard control theory terminology, it may be considered as proportional position control applied to the sensor pose under discrete tapping contacts. This control terminology was used in a more recent application of this scheme to the BRL TacTip [8]. More recently, this servo control was improved by replacing the original Bayesian predictor with a convolutional neural network to achieve controlled 2D sliding motion around various complex objects [13]. A key advance was that the neural network was tuned to be insensitive to motion-induced shear of the sensor surface, which is necessary for robust pose estimation with a soft tactile sensor such as the BRL TacTip.

The present work follows from these latter studies, which we now consider as *pose-based tactile servo* (PBTS) control. Analogously to pose-based visual servoing, a model that relates tactile images to sensor poses is used to control the sensor pose directly (Figure 2). Training this model using deep learning enables discovery of latent tactile features that are insensitive to shear, which is necessary for robust and accurate servo control using soft tactile sensors.

### B. Tactile pose estimation

In considering contact-based pose estimation, one can distinguish between tactile sensing and force/torque sensing of local object pose. A passive fingerpad attached to a force/torque sensor can detect surface pose by the method of ‘intrinsic contact sensing’ [25], which models how forces determine the contact location on the fingertip surface and the local normal to the surface under contact. This method has been improved to encompass deformable fingertips, enabling accurate tracing over curved objects via a combination of normal force control and guided transverse motion [26], [27]; moreover, the object shape can be explored with methods that implicitly model the surface [28], [29]. However, intrinsic contact sensing has not been applied to other object features such as edges, which would require the estimation of edge pose from a relatively low-dimensional force/torque signal.

Tactile arrays provide high-dimensional information about surface shape. However, there are challenges in mapping the tactile image to the local pose of an object feature: (i) for soft curved tactile sensors like our fingertips, the map from the tactile image to object feature pose will be complex and highly nonlinear; (ii) more fundamentally, for soft interactions, the tactile image depends not only on the pose of the object feature, but also the history of how that object feature was contacted, for example in the shear of the soft sensor surface as it moved into its pose [13], [30]. In our view, these difficulties have confined the use of robot touch to very primitive tasks compared with the fine motor capabilities of humans [12].

Past work on tactile servoing by Li *et al* and Kappassov *et al* avoided these problems by using a hard, planar tactile array [7], [9]. In this special case, it is possible to extract tactile features from the tactile image (*e.g.* centre of contact and

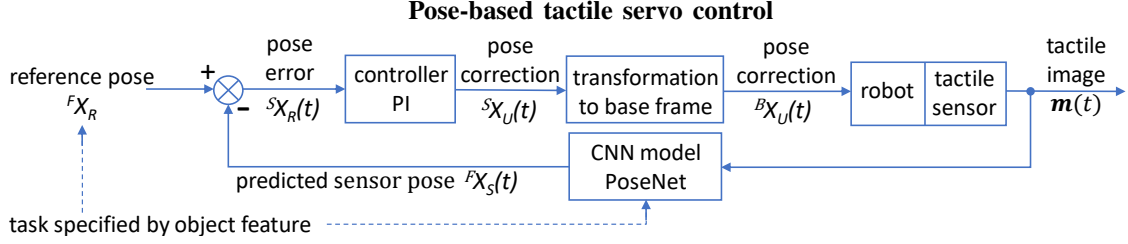


Figure 2. Pose-based tactile servo control loop with a pose error  ${}^S X_R \in \text{SE}(3)$  between the sensor pose and a reference pose that feeds into a PI controller. This controller drives a pose correction  ${}^S X_U$  of the sensor, which is transformed to the base frame  ${}^B X_U$  and sent to the robot (note that these are combined in Figure 1b). After the pose correction, the sensor acquires a new tactile image  $\mathbf{m}$  that is used to predict the sensor pose, feeding back into the pose error. The reference pose and predicted sensor pose are defined with respect to an object feature (e.g. an edge or surface), which is tracked in the servo control task.

image moments) that linearly relate to the pose of the object feature and are independent of the contact motion. However, if the tactile sensor is compliant or non-planar, as is typical of tactile sensors like our fingertips, then these simple relations do not hold. Moreover, for all tactile sensors, including planar arrays, the shape and curvature of the object features will affect the tactile image, and hence its relation to the pose.

In this paper, we apply recent progress in using deep learning with the BRL TacTip to estimate the pose of object features with a soft curved tactile sensor [12]. Specifically, deep learning can be used to train accurate ‘PoseNet’ models of object surface and edge features, such that those models are insensitive to nuisance variables including the motion-dependent shear due to soft interactions. Our method involves using representative sensor motions as unlabelled perturbations of the training data. For more background on deep learning for tactile pose estimation, we refer to [12].

### III. METHODS: ALGORITHMS

#### A. Pose-Based Tactile Servo Control

1) *Pose error*: Following a classic review of visual servo control [10], we begin with the pose error to be minimized

$$e(t) = {}^S X_R(t) = {}^S X_F(t) \cdot {}^F X_R = {}^F X_S^{-1}(t) \cdot {}^F X_R \quad (1)$$

specified as a transformation between the sensor  $S$  pose at time  $t$  and a reference pose  $R$  that will be the set-point of the controller. This error is an element  $X \in \text{SE}(3)$  of the special Euclidean group of translations and rotations, here represented in Cartesian coordinates  $(x, y, z)$  and Euler angles  $(\alpha, \beta, \gamma)$ . Then the pose error  $e = (e_x, e_y, e_z; e_\alpha, e_\beta, e_\gamma)$  is the transformation  ${}^S X_R$  to move the sensor to the reference, equivalent to specifying the reference in the coordinates of the sensor frame (using the notation in [19]).

This representation of pose as a transformation is important because in this context it is incorrect to calculate the error by subtracting two vectors. For 3D servo control, the subtraction vector can be a good approximation at small angles, but successive operations will build up undesired motions.

2) *Edge and surface features*: In practice, we consider the sensor  ${}^F X_S$  and reference  ${}^F X_R$  in the coordinates of a local feature frame  $F$  of an object. These object features are a local region of an object with a specific geometry, such as an edge or surface. (Note that these are distinct from tactile features, which are derived from the tactile image.) Feature

frames for the surface and edge are shown in Figure 3 with the coordinates used to specify the poses (Equation 2,3 below).

The choice of object feature has two roles. First, it defines the task: here servoing along an edge or over a surface. Second, it determines the tactile perception needed to estimate the sensor pose in the feature frame  ${}^F X_S(\mathbf{m})$  from tactile measurements  $\mathbf{m}$ . In this work, these measurements comprise an image of markers underneath the surface of a tactile sensor, although the formalism given here is general to any high-definition tactile sensor. In particular, we use a PoseNet convolutional neural network to predict the sensor pose in the frame of the object feature (subsection III-B).

3) *Sensor pose*: The geometry of these object features restricts which 3D components of the sensor pose can be determined from tactile measurements. For an edge parallel to the  $y$ -axis, or a surface parallel to the  $(x, y)$ -plane of the sensor frame, the 3D pose components that can be unambiguously found in the feature frame are given by the non-zero pose components as follows (Figure 3, red arrows):

$$\text{3D surface:} \quad {}^F X_S = (0, 0, z; \alpha, \beta, 0), \quad (2)$$

$$\text{3D edge:} \quad {}^F X_S = (x, 0, z; \alpha, \beta, \gamma). \quad (3)$$

The components that leave the sensor pose invariant with respect to the object feature are set to zero (Figure 3, blue arrows), as they cannot be found from tactile measurements.

In practice, these sensory invariances are idealizations that hold only for infinite straight edges or planar surfaces. Here we consider them to hold approximately on local regions of a curved edge or surface. In principle, this approximation could be improved with knowledge of the edge or surface geometry (e.g. from vision or touch), which is interesting topic for further research.

4) *Reference pose*: The reference (Equation 1) depends on the geometry of the object feature, with components in the feature frame:

$$\text{3D surface:} \quad {}^F X_R = (r_x, r_y, r_z; r_\alpha, r_\beta, r_\gamma), \quad (4)$$

$$\text{3D edge:} \quad {}^F X_R = (r_x, r_y, r_z; r_\alpha, r_\beta, r_\gamma). \quad (5)$$

These components are shown in Figure 3 along with the transformations between frames.

By comparing the sensor pose (Equations 2,3) with the reference (Equations 4,5), we see two types of error component: (i) those where both the reference and sensor pose can be non-zero, which correspond to displacing the sensor relative to the

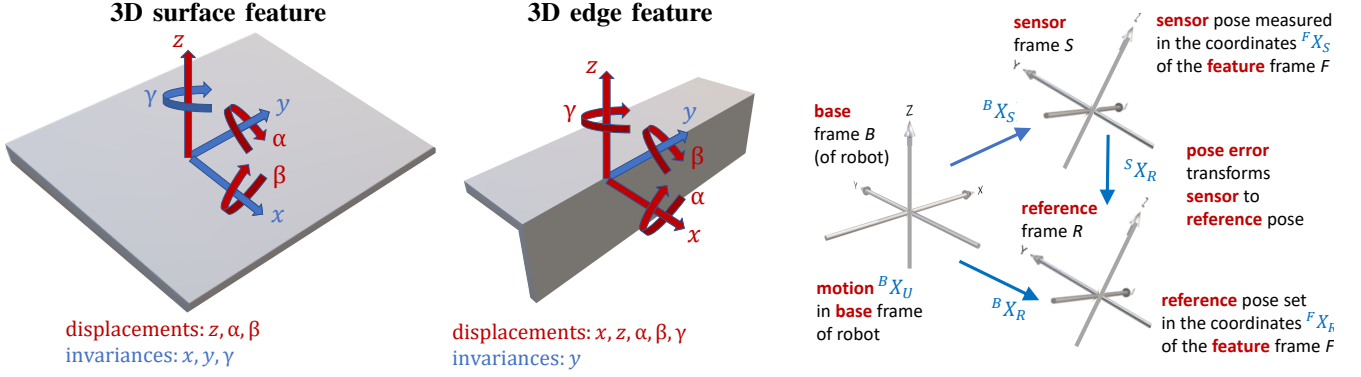


Figure 3. Edge and surface features under translations and rotations  $X = (x, y, z; \alpha, \beta, \gamma) \in \text{SE}(3)$ . Transformations that displace the feature are shown in red and invariances in blue (assuming straight edges and a flat surface).

object feature (coloured red in Figure 3 and Equations 4,5); (ii) those where just the reference can be non-zero, which correspond to trivial transformations of the sensor relative to the object feature (coloured blue in Figure 3 and Equations 4,5).

In practice, these displacements and invariances hold approximately on local regions of an object. As the sensor moves over a curved edge or surface, the sensor pose is disturbed in the feature frame on a local part of the object (which itself moves relative to the fixed base frame of the robot when the object is non-uniform). The disturbance produces a pose error, which drives the controller to move the sensor towards the reference in the new feature frame. Repeating this procedure serves the tactile sensor over a curved edge or surface.

Note that the geometry of the object feature determines how a tactile sensor can follow that feature and orient relative to the local feature frame. This is different from Li *et al.*'s approach (see subsection II-A), which composed an external motion signal with the controlled motion [7]. In principle, the reference components for the invariances could be set to zero (Equations 4,5, blue terms) and the control composed with an external signal. However, an external motion signal can disturb the pose components that are being controlled. Here we unify the two motions within a single reference, keeping complete freedom to traverse the object without disturbing the servo control (by traversing with invariances of the local feature).

5) *Controller*: It remains to specify the control law that aims to minimize the pose error in Equation 1. In this work, we control the sensor pose using a proportional-integral (PI) controller in discrete time ( $t = 0, 1, 2, \dots$ ), where we consider the output motion of the sensor in the sensor frame:

$${}^S X_U(t) = K_P {}^S X_R(t) + K_I f \left[ \sum_{t'=0}^t {}^S X_R(t') \right]. \quad (6)$$

The pose error  ${}^S X_R = (e_x, e_y, e_z; e_\alpha, e_\beta, e_\gamma)$  is treated as a 6D-vector by the controller, which aims to drive these components to zero. (Note that no Euclidean group operations are required for the controller to converge, so this is consistent mathematically.) The diagonal  $6 \times 6$  gain matrices  $K_P$  and  $K_I$  are supplemented with an anti-windup function  $f[\cdot]$  bounding the integral error between a minimum and maximum.

In our system, position control of the robot is specified in its base frame  $B$ , which is set at the start of the experiment

along with an initial sensor pose  ${}^B X_S(0)$ . The pose correction in the base frame is then given by the controller output:

$${}^B X_U(t) = {}^B X_S(t) \cdot {}^S X_U(t). \quad (7)$$

This pose correction is sent to the robot to perform the movement. Note that Equations 6,7 can be written equivalently as a controller in the base frame using  ${}^B X_R(t) = {}^B X_S(t) \cdot {}^S X_R(t)$ , consistent with Figure 1b.

6) *Implementation*: All poses  $(x, y, z; \alpha, \beta, \gamma) \in \text{SE}(3)$  are represented in Cartesian coordinates and Euler angles (in the extrinsic-xyz convention). To improve numerical stability, operations on poses were carried out after transforming from Euler angles to quaternions using standard techniques.

The sensor pose components in the feature frame (Equations 4,5) are assumed to lie within ranges:  $x \in [-5, 5]$  mm horizontally centred on the edge;  $z \in [-5, -1]$  vertically into the surface or top of the edge;  $\alpha, \beta \in [-15^\circ, 15^\circ]$  roll and pitch around the surface/edge normal; and  $\gamma \in [-45^\circ, 45^\circ]$  yaw centred on the edge (Appendix: Table II). These ranges determine the span of data used to train the neural network for predicting the sensor pose. A typical reference pose is set in center of these ranges, representing a  $-3$  mm contact depth with the sensor oriented normal to the surface or edge.

The diagonal control gain matrices (Appendix: Table IV) were tuned manually to give good overall performance while not being specific to any of our experiments. Proportional gains were 0.5 for components of the displacement (red) and 1 for invariances (blue); integral gains were 0.3 for translational and 0.1 for rotational displacements, and 0 for the invariances. The integrated error bounds were  $\pm 5$  mm for translations,  $\pm 15^\circ$  for roll and pitch, and  $\pm 45^\circ$  for yaw rotations.

## B. Pose prediction from deep learning

Pose-based tactile servo control requires an estimate of the sensor pose  ${}^F X_S(\mathbf{m}(t))$  in the frame of an edge or surface feature, from tactile measurements  $\mathbf{m}(t)$  at time  $t$ . In related work [12], we investigated how deep learning can be used to train accurate ‘PoseNet’ neural network models for estimating 3D pose from tactile images. This involved a systematic approach for selecting the best network hyperparameters, using Bayesian optimization applied to the validation loss, rather than the more common approach of hand-tuning.



This work uses the methods in [12] to gather training/validation data and train the neural network. We emphasise that the data collection involved a transverse sliding motion prior to recording each tactile image via an (unlabelled) random displacement of the sensor. This is important because contact-dependent shear affects measurements from optical tactile sensors such as the one used here [13], [30].

We refer to [12] for the details of the methods, and report the differences from that previous analysis. These were: (i) larger training/validation datasets of 5000/5000 samples over the same ranges as previously (Appendix: Table II); (ii) fewer iterations (100) for the hyperparameter optimization by fixing values that were consistently optimized [12], such as having 5 convolutional and 1 dense layer (Appendix: Table III).

The accuracies of these surface and edge PoseNets are reported below (Table I). The horizontal and yaw pose accuracies were much improved over previous results [12]; other pose parameters have similar or slightly poorer accuracies, which we attribute to unimportant differences in the sensor and its placement during data collection. The key point is that this method gives accurate pose estimates that are insensitive to shear as the sensor interacts with an object.

Parameter	Surface (MAE)	Range	Edge (MAE)	Range
horizontal, $x$	-	-	0.3 mm	10 mm
vertical, $z$	0.1 mm	4 mm	0.2 mm	4 mm
roll, $\alpha$	0.4°	30°	1.2°	30°
pitch, $\beta$	0.5°	30°	2.4°	30°
yaw, $\gamma$	-	-	4.1°	90°

Table I

POSENET ACCURACY: MEAN ABSOLUTE ERROR (MAE) OF PREDICTIONS. TESTS WERE PERFORMED OVER AN INDEPENDENT SET OF 2000 SAMPLES.

#### IV. METHODS: TACTILE ROBOTIC SYSTEM

##### A. Tactile sensor

This study involves the use of a soft biomimetic optical tactile sensor from the BRL TacTip family [14], [15]. The use of 3D-printing enables the designs to be highly customizable, encompassing stand-alone sensors of various shapes and sizes [15] and tactile fingertips integrated into the distal phalanges of robot hands [31], [32]. Printing multiple materials in one piece allows combination of a rigid casing (VeroWhite) with a soft sensing surface (TangoBlack). The version used here has a soft tactile dome (40 mm dia.) with 127 internal pins tipped by printed white markers that function as tactile elements, which is a standard design used in our lab [15].

An important aspect of the soft biomimetic design is that the sensor is highly sensitive to shear deformation, which induces a global movement of all pins along the direction of lateral strain in the sensing surface. While this is useful for detecting phenomena such as slip [33], it causes issues for tactile servoing when sliding over object surfaces [13], [30]. The problem is that the tactile image will depend not only on the pose of the object but also on the prior transverse movement of the sensor. As shown in previous work [13], this causes the tactile servoing to fail under sliding motion unless the pose can be inferred accurately. As described above (subsection III-B), here we mimic the effect of this transverse motion during training data collection, so that the PoseNet can be trained to be insensitive to sensor motion.

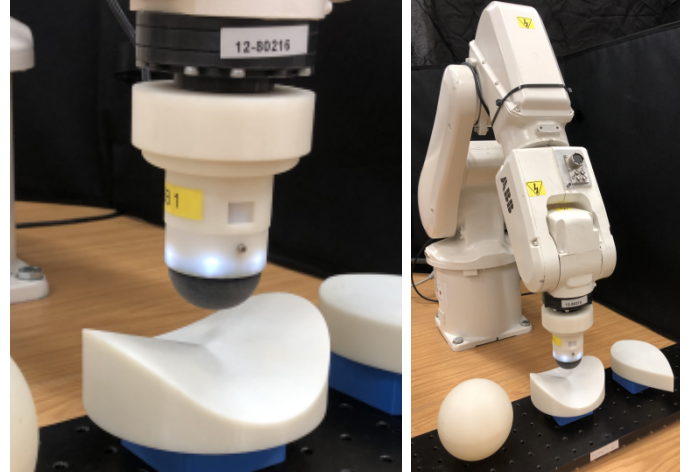


Figure 4. Tactile robotic system, showing (left) a close-up of the tactile sensor and (right) a view of the sensor-arm system next to some test objects.

##### B. Tactile robot

The TacTip optical tactile sensor is mounted as an end-effector on an industrial robot arm (Figure 4), which was also used in earlier studies of control using this tactile sensor [8], [13], [30]. We use an IRB 120 (ABB Robotics): a fairly small 6-axis industrial robot arm (reach 0.58 m, 25 kg weight, 3 kg payload) with accurate positioning (0.01 mm accuracy,  $\sim 1$  sec cycle time). The TacTip base is bolted onto a mounting plate attached to the rotating (wrist) section of the arm.

Closed-loop control of this robot is limited to long latencies ( $\gtrsim 100$  ms), since the IRB 120 is aimed at applications where its end-effector passes through predefined waypoint poses. Therefore, we control the arm in discrete updates of the end-effector pose, with the industrial robot controller (IRC5) calculating the motion between poses. While this setup is primitive compared with many research robots, *e.g.* cobots that react to humans in real-time, it does provide a basic platform sufficient for investigating pose-based tactile servo control.

##### C. Software infrastructure

The software and hardware are integrated with four main components written mainly in Python: (1) Tactile images are collected using the OpenCV library, then preprocessed and saved for training, or used directly for prediction; (2) These images are cropped, thresholded and subsampled in OpenCV to give  $(128 \times 128)$ -pixel images, which are then passed to the deep learning models implemented using the Keras deep learning library; (3) The resulting predictions are passed to control software in Python (with some visualizations using the MATLAB Engine API); (4) Finally, the computed control signal is sent to the robot arm via the RAPID API.

Training and optimization of the deep neural networks was implemented on a Titan Xp GPU hosted on a Windows 10 PC. A training run typically takes about 10 minutes. The learnt model is then copied to the robot control PC, which in this case was a Windows 10 PC with limited GPU hardware. Even so, the PoseNet models typically made predictions in about 50 msec. The longest delay within the cycle was the latency between the control PC and the robot arm (typically 100 ms).

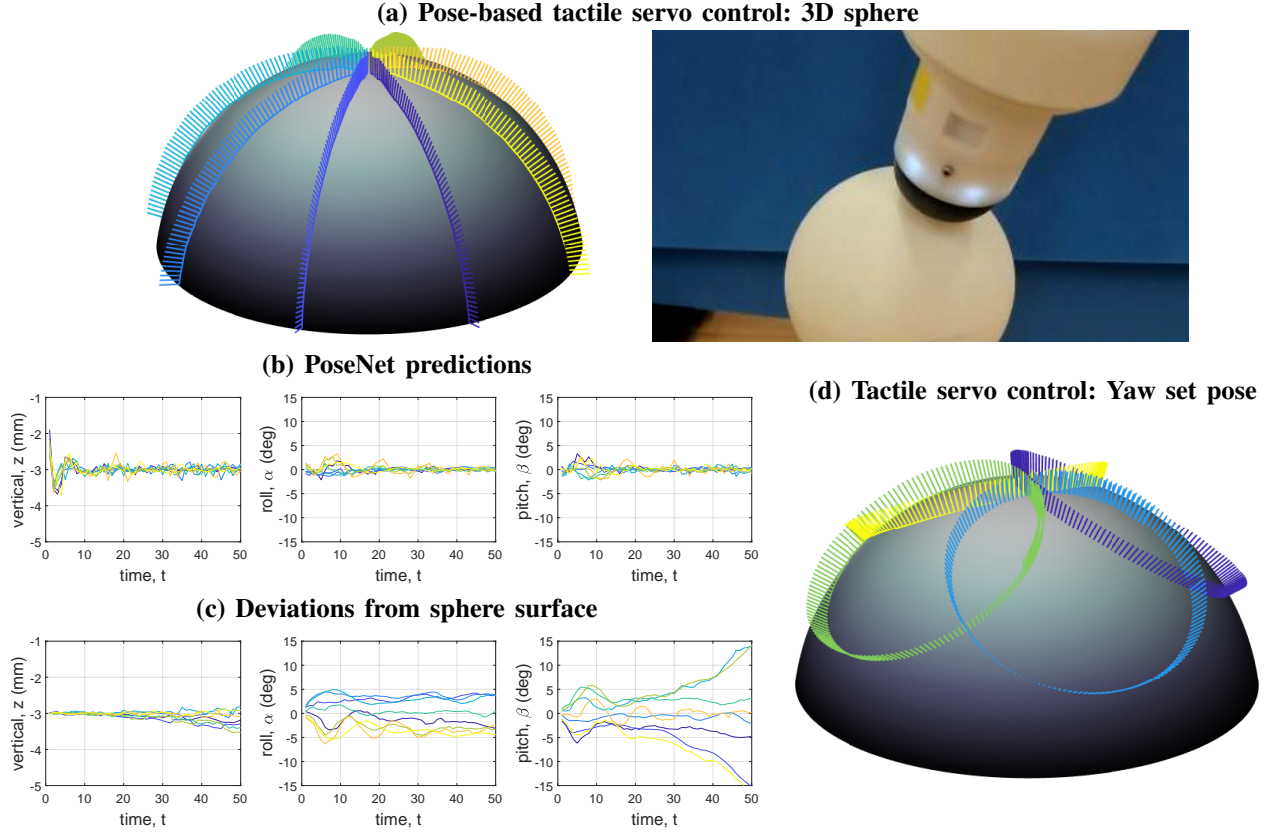


Figure 5. Pose-based servo control over a sphere. (a) Trajectories with predicted surface normals ( $z$ -axis) are shown for 8 reference poses with angles  $(r_x, r_y) = (\cos \varphi, \sin \varphi)$  every  $45^\circ$ . The corresponding PoseNet predictions (b) and deviations from the surface (c) are plotted against time. (d) Trajectories when the yaw reference is non-zero,  $r_\gamma = 2^\circ$ , at angles  $\varphi = 0^\circ, 90^\circ, 180^\circ, 270^\circ$ . A video for the 8 reference poses is in Supplementary Movie S1

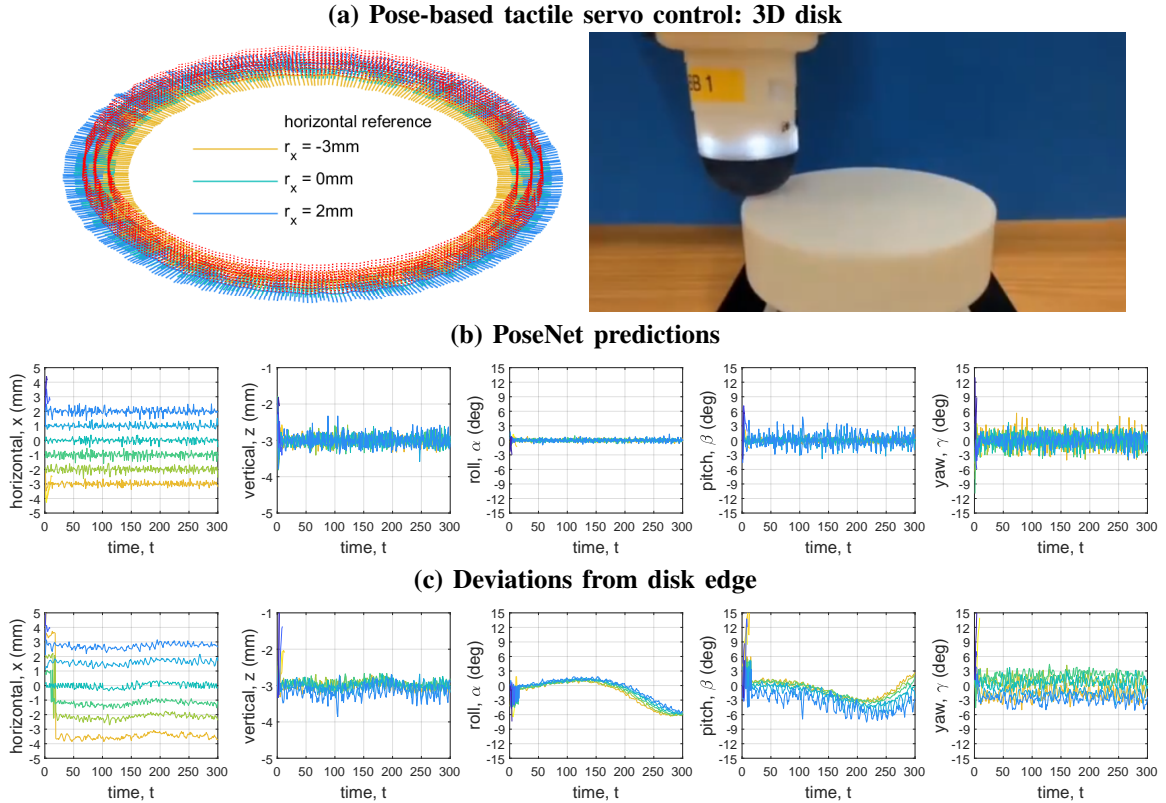


Figure 6. Pose-based servo control around a disk edge. (a) Trajectories for 3 reference poses  $r_x = -3, 0, 3$  mm with predicted surface normals and edge normals, (b) PoseNet predictions and (c) deviations from the disk edge for reference poses over  $[-3, 2]$  mm. A video is in Supplementary Movie S2.

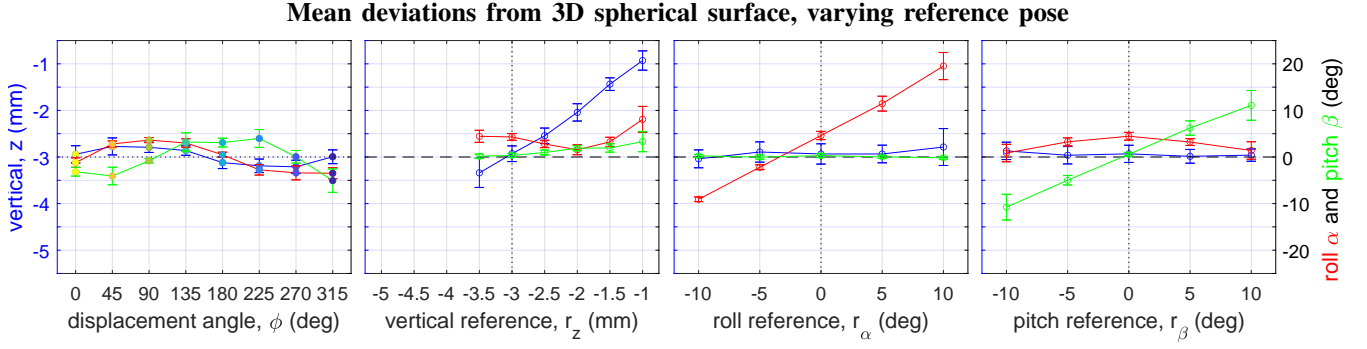


Figure 7. Effect of changing the reference pose on PBTS control for the spherical surface. The mean deviations and spreads (1 s.d.) of the pose deviations are calculated over a trajectory over the surface of a sphere, with deviations coloured according to their pose component (shown on the left and right axes). The coloured markers for  $\varphi$  correspond to the trajectories in Figure 5 (panels a-c).

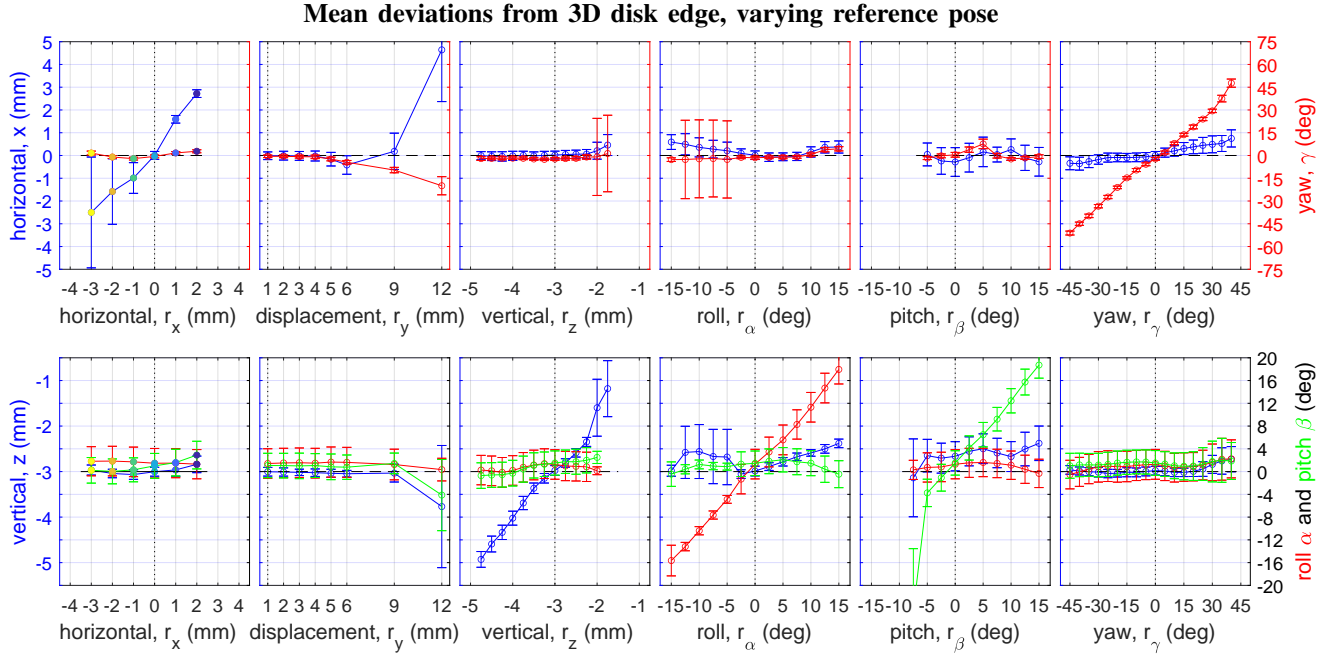


Figure 8. Effect of changing the reference pose on PBTS control for the 3D disk, showing (a) the horizontal and yaw deviations; and (b) the vertical, roll and pitch deviation. The mean deviations and spreads ( $\pm 1$  s.d.) are calculated over a trajectory around the disk, with deviations coloured according to their pose component (shown on the axes). The coloured markers for  $r_x$  correspond to the trajectories in Figure 6.

## V. RESULTS: SERVO CONTROL ON REGULAR OBJECTS

### A. 3D spherical surface

First, the pose-based servo control was tested on a 3D spherical surface, starting at the apex and moving outwards and downwards. A contact depth of  $-3$  mm and step size of  $1$  mm over the surface in a direction at angle  $\varphi$  while maintaining the sensor normal to the surface was set with a reference pose  ${}^F X_R = (\cos \varphi, \sin \varphi, -3; 0, 0, 0)$ .

The resulting trajectories followed the sphere surface accurately after initially aligning the sensor to the surface (Figure 5a, coloured by angle  $\varphi = 0^\circ, 45^\circ, \dots, 315^\circ$ ). The PoseNet predictions match the estimated deviations with a small bias of a few degrees in the roll and pitch deviations and a vertical deviation of less than  $0.1$  mm for the first  $30$  mm-steps, then drifting up to around  $0.4$  mm and a large deviation in pitch (Figure 5b,c). From inspection, the sensor measurements seem to depend on gravity, with the markers moving downwards as

the tip is oriented horizontally. We therefore attribute this drift to gravity deforming the sensor tip as it orients horizontally relative to the more vertical pose during training.

We also considered servo control with reference poses  ${}^F X_R = (\cos \varphi, \sin \varphi, -3; 0, 0, 2)$  that rotate the sensor in  $\gamma = 2^\circ$  steps while moving over the surface (Figure 5d). The accuracy is visible in the way that the trajectories close at the apex of the sphere rather than drift away from perfect circles.

Performance over each trajectory was summarized by the mean and spread of the vertical, roll and pitch ( $z, \alpha, \beta$ ) deviations from the normal to the surface (Figure 7). These deviations from the sphere, although small, appear periodic in the angle  $\varphi$  that sets the direction of the trajectory (Figure 7b, left panel). This periodicity is consistent with the effect of gravity deforming the sensor, since the trajectory angle determines which part of the sensing surface points upwards and hence the orientation of the roll and pitch.

The servo control was then tested over reference poses



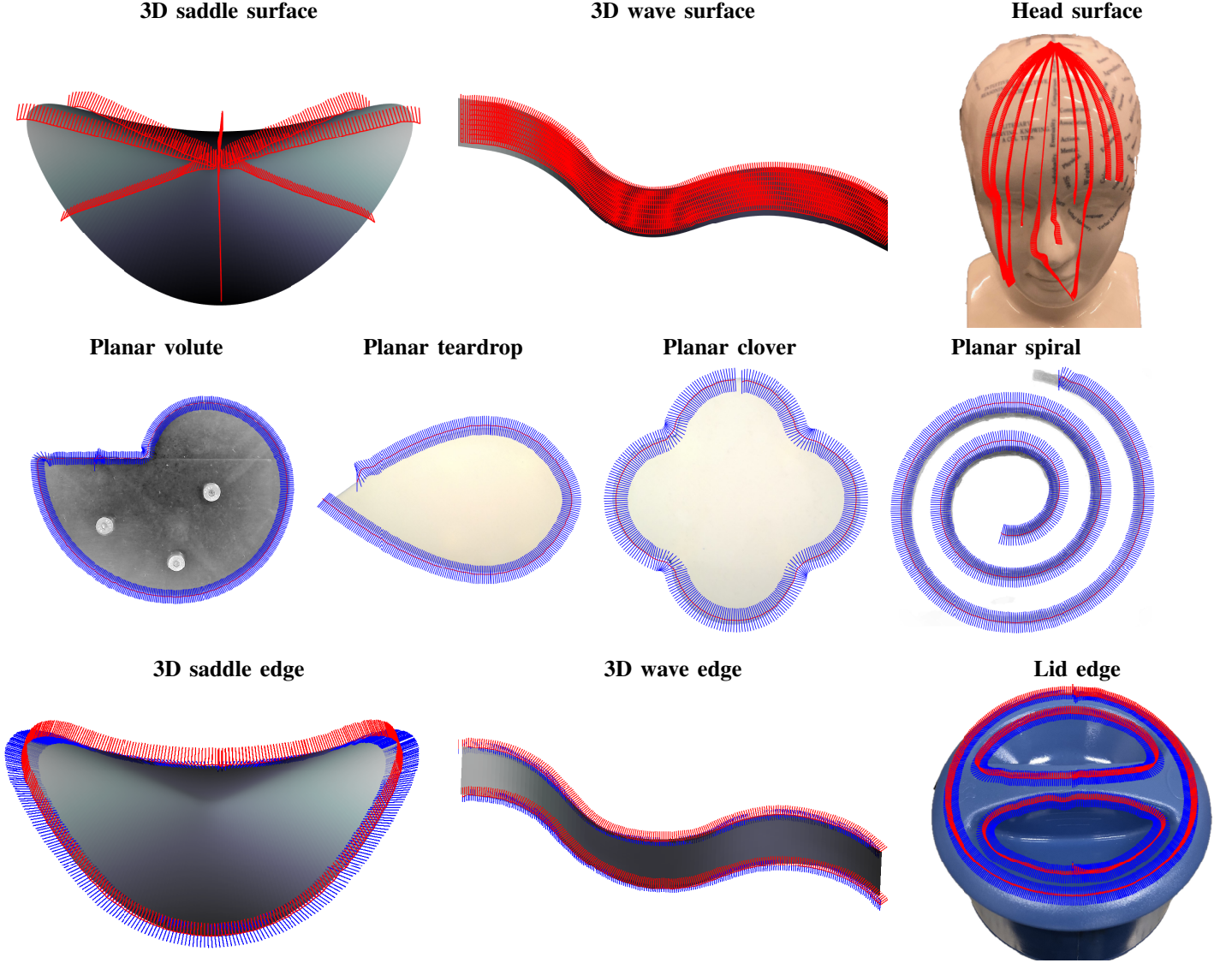


Figure 9. Pose-based control over irregular objects, following 3D surfaces (top row), planar edges (middle row) and 3D contours (bottom row). Predicted surface normals ( $z$ -axis, red) and edge normals ( $x$ -axis, blue) are shown. All objects were novel because the PoseNet was trained on the disk. Supplementary videos are in Movie S3 (planar edged objects), Movie S5 (wave edge and surface), Movie S6 (saddle edge and surface), Movie S7 (head) and Movie S8 (lid).

${}^F X_R = (1, 0, r_z; r_\alpha, r_\beta, 0)$  ranging in contact depth, roll and pitch. Overall, the servoing remained accurate, with small vertical deviations of  $\lesssim 0.2$  mm and small angular deviations of  $(\alpha, \beta) \lesssim (5^\circ, 0^\circ)$ . The deviation also varied linearly with its corresponding reference component (Figure 7b, right panels). Overall, the servo control has the expected effect on the deviations of the trajectories from the true surface normals.

### B. 3D disk edge

Pose-based servo control was then tested on a planar disk. A contact depth of  $-3$  mm and step-size of  $1$  mm along the edge with sensor normal to the disk was set with a reference pose  ${}^F X_R = (0, 1, -3; 0, 0, 0)$ .

The resulting trajectory precisely followed the outside of the disk after an initial motion to align the sensor to the edge (Figure 6, green trajectory). The PoseNet predictions match the estimated deviations from the edge to  $\lesssim 0.3$  mm horizontally,  $\lesssim 0.2$  mm vertically and  $\lesssim 3^\circ$  yaw. There is an

apparent periodic deviation in the roll and pitch (Figure 6c). An inspection revealed the sensor was mounted slightly off-normal to the wrist, which caused it to precess as the wrist rotated. This inaccurate mounting was corrected by the servo control to give an apparent deviation in roll and pitch.

Tactile servoing around the 3D disk was then examined over a range of reference poses  ${}^F X_R = (r_x, r_y, r_z; r_\alpha, r_\beta, r_\gamma)$ , with the performance over each trajectory summarized by the mean and spread of the deviation from the disk edge. The servoing remained accurate over these ranges, with variations in each reference component mainly affecting only the corresponding pose component in a linear manner (Figure 8).

Both the 3D edge and sphere had similar deviations along the vertical, roll and pitch with changing the reference components. Vertical deviations were more accurate for the edge than the surface, even though the surface PoseNet is more accurate than the edge PoseNet. We attribute this to the effects of gravity on the sensor tip (as described in subsection V-A).



### 3D compliant surface: squishy brain

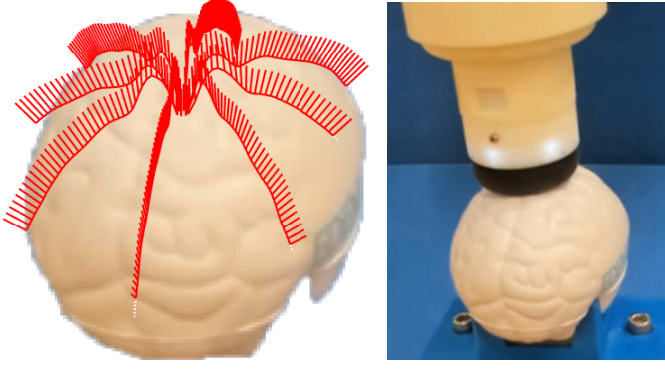


Figure 10. Pose-based control over a soft object (a ‘squishy brain’; trajectories angled every  $45^\circ$ ). Both the object and sensor deform initially before the sensor maintains a light touch. A video is in Supplementary Movie S9.

## VI. RESULTS: SERVO CONTROL ON IRREGULAR OBJECTS

### A. Irregular 3D surfaces

Pose-based servo control was next trialled on several irregular 3D shapes: a saddle, a 3D wave and a complex surface (a model of a head). As the 3D PoseNet was trained on a planar surface, successful tests demonstrated its robustness to moderately curved surfaces.

All irregular surfaces were successfully traced (Figure 9, top row). The close match of the trajectories to the the objects is seen by overlaying the motion over the design of the saddle and wave, and observing the likeness to a photographic image of the head. (Note that some paths were shorter because of a singularity in the robot’s workspace on the right eye socket.)

### B. Irregular planar edges

The next trials were on a range of irregular planar shapes: a volute, teardrop, clover and spiral. The success of these tests demonstrated robustness to positive and negative edge curvatures, including corners.

All irregular planar contours closely matched the true shapes, in comparison to the underlaid photos of the objects (Figure 9, middle row). There was a failure mode at very sharp corners where the 3D controller could not complete the teardrop point and the inward tip of the spiral. Near these points, large deviations in roll and pitch occurred that took the sensor away from the vertical (Supplementary Movie S3).

However, the PoseNet model was only trained on edges, so any success on a corner (such as the two on the planar volute) is an emergent property of the control. Further, for sensor motion constrained to maintain a vertical orientation, all contours were successfully traced (Supplementary Movie S4), as also found in previous work on 2D servo control [13].

### C. Irregular 3D edges

Trials were then around several irregular 3D contoured shapes: the edges of the 3D wave and saddle used as surfaces above, and a complex contoured object (a container lid). The success of these tests demonstrated robustness to varying edge curvatures and profiles.

All plotted contours closely followed the shapes of the irregular 3D objects (Figure 9, bottom row). This is visible in overlays of the 3D designs of the saddle and wave, and the good likeness to the image of the complex-shaped lid. We draw particular attention to the accurate tracing of the lid, which was challenging because its ‘edge’ was much blunter than the one used in training.

### D. Irregular compliant 3D surface

The final tests of pose-based servo control were on a soft object: a ‘squishy brain’. The sensor was initially placed at a location where the object was deformed and then servoed to make a gentler contact while tracing the object surface.

The resulting trajectories traced the surface of the squishy brain (Figure 10) while also having a physical interaction where the sensor bounces back from the surface while the object returns to its undeformed shape. This complex dynamic interaction depends on the material properties of the sensor skin and the object, along with the dynamics of the servo control. The interaction of servo control with soft and flexible objects is a rich, open-ended topic for further investigation.

## VII. DISCUSSION

In this paper, we began by reviewing tactile servo control and pose estimation, distinguishing image-based and pose-based control (section II). We then formalised pose-based tactile servo control by blending classic concepts from visual servoing with tactile sensing using a PoseNet deep neural network for pose estimation (section III). Our test robot comprised the BRL TacTip mounted on an industrial robot arm (section IV). These methods were validated with a quantitative assessment of tactile servoing performance on known regular objects (a sphere and disk) under changes in control parameters (section V). We then demonstrated accurate servo control over many novel irregular objects, including a saddle, wave, several planar edges, a container lid, a bust of a human head and a squishy brain (section VI).

*Generality of the approach:* How broad a range of objects does our method of servo control apply to? Many different test shapes were accurately traced (Figure 9), using training data from just the edge and centre of a flat 3D-printed disk. The controller only struggled when the object became very curved. Although a soft sensor of this size (40 mm dia. dome) cannot fully contact sharply concave surface features such as the base of the nose of the porcelain bust, this did not cause the servo control to fail (Supplementary Movie S7).

The test surfaces varied in roughness, from smooth perspex and glazed porcelain to a textured plastic lid and 3D-printed stimuli. However, we did not notice any dependence of the servo control on roughness. In our view, this was because the effect of roughness was to change the shear on the sensor surface, and the PoseNets were trained to be insensitive to shear. For an initial test on a soft object, we tried tactile servoing over a ‘squishy brain’ (Figure 10). The dynamics of the soft tactile sensor were found to be coupled to the object deformation, which is a rich topic for further investigation.

*Pose-based vs image-based servo control:* In our opinion, conceptualising tactile servo control as pose-based or image-based will help the research field of robot touch to progress. This terminology clarifies the relation with visual servo control, where the partition into IBVS and PBVS has been instrumental for robot vision from the 1990s onwards.

An apparent difference between PBTS and PBVS control is that the model of object pose from the visual image usually applies to the global pose of an object, whereas we model the local pose of an object feature such as a surface or edge. This difference arises from how the sensors are used: touch is a proximal sense that can only contact part of an object, whereas vision is a distal sense that can view an entire object. However, one could interpret the entire visual object as providing local features within a global scene, which are more like the local features in touch. Also, visual servo control applies to scanning over local features of objects such as contours, which is closer to human vision where the eye moves a small, high-resolution fovea to actively explore an object or scene.

*Benefits for haptic exploration and manipulation:* Haptic exploration refers to how the human hand (and brain) is used to recognize surfaces and objects. Classic work by psychologists Lederman and Klatzky on exploratory procedures for haptic object recognition [34] motivated robot studies of exploring an unknown environment using artificial fingertips [35], [36]. Robot haptic exploration encompasses using fingertips to slide over surfaces [22], [26], [36], tap around contours [8], [23], [24], slide around contours [5], [13], roll objects in-hand [37], [38] and enclose an object in-hand [39], [40]. All of these robot exploratory procedures would benefit from precise control of the fingertip pose against the object.

Manipulation is inherently coupled with exploration, as explained by Okamura and Cutkowsky [36]: purposeful movement of an object requires a model for motion planning that can be acquired through exploration; in turn, exploration requires manipulation of the object. During exploration, two or more fingers can stabilize or roll an object while other fingers travel over the object surface [38]. Again, this requires the fingers be precisely controlled relative to the object surface.

## VIII. CONCLUSION

The pose-based tactile servo control described here enables a range of competencies that allow robots to interact physically with their environments. This includes any task that involves precise control of a soft tactile-sensorized part of a robot; for example, a soft fingertip to have a desired pose relative to a surface, edge or other local object feature. This control can enable tactile probes to accurately explore and map objects or surfaces; also those probes can be used as non-prehensile manipulators to push or reposition objects. The control could also guide the precise use of fingertips on a robot hand to stabilize and explore held objects, which is a necessary component of in-hand manipulation. The ultimate aim of controlled soft touch such as pose-based tactile servo control is to provide a route towards an ease of dexterity that any manual task currently done by humans could be automated.

## SUPPLEMENTARY MATERIAL

Movie S1 - Sphere surface [youtu.be/PrtpVU-alrk](https://youtu.be/PrtpVU-alrk)  
 Movie S2 - Disk edge [youtu.be/UXIM8k3Pjqs](https://youtu.be/UXIM8k3Pjqs)  
 Movie S3 - Planar edged objects) [youtu.be/NldNjDKNS-I](https://youtu.be/NldNjDKNS-I)  
 Movie S4 - Planar edged objects (2D) [youtu.be/nlFep15iZdE](https://youtu.be/nlFep15iZdE)  
 Movie S5 - Wave edge & surface [youtu.be/7CfnEZGgBRc](https://youtu.be/7CfnEZGgBRc)  
 Movie S6 - Saddle edge and surface [youtu.be/QC3Q6ArYoUE](https://youtu.be/QC3Q6ArYoUE)  
 Movie S7 - Head surface [youtu.be/N98nVqXvm88](https://youtu.be/N98nVqXvm88)  
 Movie S8 - Lid edges [youtu.be/x-xnLj\\_RgAk](https://youtu.be/x-xnLj_RgAk)  
 Movie S9 - Squishy brain surface [youtu.be/BWrq5z0dLf4](https://youtu.be/BWrq5z0dLf4)  
 Linked as YouTube videos <https://youtu.be/...>

## APPENDIX

Training data parameters, control parameters and PoseNet parameters used in this work are given in Tables II-IV.

## ACKNOWLEDGMENT

The authors thank Andy Stinchcombe and other members of the BRL Tactile Robotics group. We thank Nvidia for the donation of the Titan Xp GPU used for this research. This work was supported by an award from the Leverhulme Trust on ‘A biomimetic forebrain for robot touch’ (RL-2016-39).

## REFERENCES

- [1] Leon D. Harmon. Automated Tactile Sensing. *The International Journal of Robotics Research*, 1(2):3–32, June 1982.
- [2] Zhanat Kappassov, Juan-Antonio Corrales, and Véronique Perdereau. Tactile sensing in dexterous robot hands — Review. *Robotics and Autonomous Systems*, 74:195–220, December 2015.
- [3] Shan Luo, Joao Bimbo, Ravinder Dahiya, and Hongbin Liu. Robotic tactile perception of object properties: A review. *Mechatronics*, 48:54–67, December 2017.
- [4] Alan D Berger and Pradeep K Khosla. Using Tactile Data for Real-Time Feedback. *The International Journal of Robotics Research*, 10(2):88–102, April 1991.
- [5] Ning Nicholas Chen, Hong Zhang, and R. E. Rink. Edge tracking using tactile servo. In *Proceedings 1995 IEEE/RSJ International Conference on Intelligent Robots and Systems*, volume 2, pages 84–89, Pittsburgh, PA, USA, 1995.
- [6] Hong Zhang and Ning Nicholas Chen. Control of contact via tactile sensing. *IEEE Trans. Robot. Automat.*, 16(5):482–495, October 2000.
- [7] Qiang Li, Carsten Schürmann, Robert Haschke, and Helge Ritter. A Control Framework for Tactile Servoing. In *Robotics: Science and Systems IX*. Robotics: Science and Systems Foundation, June 2013.
- [8] Nathan F. Lepora, Kirsty Aquilina, and Luke Cramphorn. Exploratory Tactile Servoing With Active Touch. *IEEE Robot. Autom. Lett.*, 2(2):1156–1163, April 2017.
- [9] Zhanat Kappassov, Juan-Antonio Corrales, and Véronique Perdereau. Touch driven controller and tactile features for physical interactions. *Robotics and Autonomous Systems*, 123:103332, January 2020.
- [10] Francois Chaumette and Seth Hutchinson. Visual servo control. I. Basic approaches. *IEEE Robot. Automat. Mag.*, 13(4):82–90, December 2006.
- [11] Pavan Sikka, Hong Zhang, and Steve Sutphen. Tactile servo: Control of touch-driven robot motion. In Tsuneo Yoshikawa and Fumio Miyazaki, editors, *Experimental Robotics III*, volume 200, pages 219–233. Springer-Verlag, London, 1994.
- [12] Nathan F. Lepora and John Lloyd. Optimal Deep Learning for Robot Touch: Training Accurate Pose Models of 3D Surfaces and Edges. *IEEE Robot. Automat. Mag.*, 27(2):66–77, June 2020.
- [13] Nathan F. Lepora, Alex Church, Conrad de Kerckhove, Raia Hadsell, and John Lloyd. From Pixels to Percepts: Highly Robust Edge Perception and Contour Following Using Deep Learning and an Optical Biomimetic Tactile Sensor. *IEEE Robot. Autom. Lett.*, 4(2):2101–2107, April 2019.
- [14] Craig Chorley, Chris Melhuish, Tony Pipe, and Jonathan Rossiter. Development of a Tactile Sensor Based on Biologically Inspired Edge Encoding. In *International Conference on Advanced Robotics*, pages 1–6, 2009.

object feature	samples	pose range (labelled)	displacement range (unlabelled)
3D surface	10000	(0, 0, [-5, -1]; $\pm 15, \pm 15, 0$ )	( $\pm 5, \pm 5, 0; \pm 5, \pm 5, \pm 5$ )
3D edge	10000	( $\pm 5, 0, [-5, -1]; \pm 15, \pm 15, \pm 45$ )	( $\pm 5, \pm 5, 0; \pm 5, \pm 5, \pm 5$ )

Table II  
TRAINING/VALIDATION DATA PARAMETERS (UNITS: MM, MM, MM; DEG, DEG, DEG).

object feature	# conv. layers	# dense layers	batch norm.	# conv. kernels	# dense units	batch size	activation function	dropout coef.	L1-reg. coef.	L2-reg. coef.
3D surface	5	1	None	256	256	16	ELU	0.0047	0.0001	0.0159
3D edge	5	1	None	256	256	16	ReLU	0.0700	0.0001	0.0019

Table III  
POSENET PARAMETERS. THE FIRST 6 PARAMETERS WERE FIXED (USING VALUES FROM [12]); THE FINAL 4 PARAMETERS WERE OPTIMIZED.

object feature	sensor pose ${}^F X_S$	reference pose ${}^F X_R$	proportional gain $K_P$	integral gain $K_I$	integral bounds $B$
3D surface	(0, 0, z; $\alpha, \beta, 0$ )	(0, 1, -3; 0, 0, 0)	(1, 1, $\frac{1}{2}; \frac{1}{2}, \frac{1}{2}, 1$ )	(0, 0, $\frac{3}{10}; \frac{1}{10}, \frac{1}{10}, 0$ )	$\pm(0, 0, 5; 15, 15, 0)$
3D edge	(x, 0, z; $\alpha, \beta, \gamma$ )	(0, 1, -3; 0, 0, 0)	( $\frac{1}{2}, 1, \frac{1}{2}; \frac{1}{2}, \frac{1}{2}, \frac{1}{2}$ )	( $\frac{3}{10}, 0, \frac{3}{10}; \frac{1}{10}, \frac{1}{10}, \frac{1}{10}$ )	$\pm(5, 0, 5; 15, 15, 45)$

Table IV  
POSE-BASED SERVO CONTROL PARAMETERS (UNITS: MM, MM, MM; DEG, DEG, DEG).

- [15] Benjamin Ward-Cherrier, Nicholas Pestell, Luke Cramphorn, Benjamin Winstone, Maria Elena Giannaccini, Jonathan Rossiter, and Nathan F. Lepora. The TacTip Family: Soft Optical Tactile Sensors with 3D-Printed Biomimetic Morphologies. *Soft Robotics*, 5(2):216–227, April 2018.
- [16] J. Hill and W. T. Park. Real time control of a robot with a mobile camera. In *Proc. 9th ISIR*, volume 5, pages 233–246, Washington, D.C., March 1979.
- [17] Bernard Espiau, Francois Chaumette, and Patrick Rives. A new approach to visual servoing in robotics. *IEEE Transactions on Robotics and Automation*, 8(3):313–326, June 1992.
- [18] William J. Wilson, Carol C. Williams Hulls, and Graham S. Bell. Relative end-effector control using Cartesian position based visual servoing. *IEEE Trans. Robot. Automat.*, 12(5):684–696, October 1996.
- [19] Seth Hutchinson, Gregory D. Hager, and Peter Corke. A tutorial on visual servo control. *IEEE Trans. Robot. Automat.*, 12(5):651–670, October 1996.
- [20] Ezio Malis, Francois Chaumette, and Sylvie Boudet. 2 1/2 D visual servoing. *IEEE Trans. Robot. Automat.*, 15(2):238–250, April 1999.
- [21] Jae S. Son and Robert D. Howe. Tactile sensing and stiffness control with multifingered hands. In *Proceedings of IEEE International Conference on Robotics and Automation*, volume 4, pages 3228–3233, Minneapolis, MN, USA, 1996.
- [22] Qiang Li, Robert Haschke, and Helge Ritter. A visuo-tactile control framework for manipulation and exploration of unknown objects. In *2015 IEEE-RAS 15th International Conference on Humanoid Robots (Humanoids)*, pages 610–615, Seoul, South Korea, November 2015. IEEE.
- [23] Uriel Martinez-Hernandez, Tony J. Dodd, Lorenzo Natale, Giorgio Metta, Tony J. Prescott, and Nathan F. Lepora. Active contour following to explore object shape with robot touch. In *2013 World Haptics Conference (WHC)*, pages 341–346, Daejeon, April 2013.
- [24] Uriel Martinez-Hernandez, Tony J. Dodd, Mathew H. Evans, Tony J. Prescott, and Nathan F. Lepora. Active sensorimotor control for tactile exploration. *Robotics and Autonomous Systems*, 87:15–27, January 2017.
- [25] Antonio Bicchi, J. Kenneth Salisbury, and David L. Brock. Contact Sensing from Force Measurements. *The International Journal of Robotics Research*, 12(3):249–262, June 1993.
- [26] Hongbin Liu, Xiaojing Song, Joao Bimbo, Lakmal Seneviratne, and Kaspar Althoefer. Surface material recognition through haptic exploration using an intelligent contact sensing finger. In *2012 IEEE/RSJ International Conference on Intelligent Robots and Systems*, pages 52–57, Vilamoura-Algarve, Portugal, October 2012.
- [27] Hongbin Liu, Kien Cuong Nguyen, Véronique Perdureau, Joao Bimbo, Junghwan Back, Matthew Godden, Lakmal D. Seneviratne, and Kaspar
- [28] Carlos Rosales, Federico Spinelli, Marco Gabiccini, Claudio Zito, and Jeremy L. Wyatt. GPAtlasRRT: A Local Tactile Exploration Planner
- Althoefer. Finger contact sensing and the application in dexterous hand manipulation. *Auton Robot*, 39(1):25–41, June 2015.
- for Recovering the Shape of Novel Objects. *Int. J. Human. Robot.*, 15(01):1850014, February 2018.
- [29] Danny Driess, Daniel Hennes, and Marc Toussaint. Active Multi-Contact Continuous Tactile Exploration with Gaussian Process Differential Entropy. In *2019 International Conference on Robotics and Automation (ICRA)*, pages 7844–7850, Montreal, QC, Canada, May 2019.
- [30] Kirsty Aquilina, David A. W. Barton, and Nathan F. Lepora. Shear-invariant Sliding Contact Perception with a Soft Tactile Sensor. In *2019 International Conference on Robotics and Automation (ICRA)*, pages 4283–4289, Montreal, QC, Canada, May 2019.
- [31] Nicholas Pestell, Luke Cramphorn, Fotios Papadopoulos, and Nathan F. Lepora. A Sense of Touch for the Shadow Modular Grasper. *IEEE Robot. Autom. Lett.*, 4(2):2220–2226, April 2019.
- [32] Jasper W. James, Alex Church, Luke Cramphorn, and Nathan F. Lepora. Tactile Model O: Fabrication and testing of a 3d-printed, three-fingered tactile robot hand. *Soft Robotics*, 2020. arXiv: 1907.07535.
- [33] Jasper Wollaston James, Nicholas Pestell, and Nathan F. Lepora. Slip Detection With a Biomimetic Tactile Sensor. *IEEE Robot. Autom. Lett.*, 3(4):3340–3346, October 2018.
- [34] Susan J. Lederman and Roberta L. Klatzky. Hand movements: A window into haptic object recognition. *Cognitive Psychology*, 19(3):342–368, July 1987.
- [35] Peter K. Allen. Mapping haptic exploratory procedures to multiple shape representations. In *Proceedings., IEEE International Conference on Robotics and Automation*, pages 1679–1684, Cincinnati, OH, USA, 1990.
- [36] Allison M. Okamura and Mark R. Cutkosky. Feature Detection for Haptic Exploration with Robotic Fingers. *The International Journal of Robotics Research*, 20(12):925–938, December 2001.
- [37] Hitoshi Maekawa, Kazuo Tanie, and Kiyoshi Komoriya. Tactile sensor based manipulation of an unknown object by a multifingered hand with rolling contact. In *Proceedings of 1995 IEEE International Conference on Robotics and Automation*, volume 1, pages 743–750, Nagoya, Japan, 1995.
- [38] Allison M. Okamura, Michael L. Turner, and Mark R. Cutkosky. Haptic exploration of objects with rolling and sliding. In *Proceedings of International Conference on Robotics and Automation*, volume 3, pages 2485–2490, Albuquerque, NM, USA, 1997.
- [39] Nicolas Gorges, Stefan Escaida Navarro, Dirk Goger, and Heinz Worn. Haptic object recognition using passive joints and haptic key features. In *2010 IEEE International Conference on Robotics and Automation*, pages 2349–2355, May 2010.
- [40] Nicolas Sommer and Aude Billard. Multi-contact haptic exploration and grasping with tactile sensors. *Robotics and Autonomous Systems*, 85:48–61, November 2016.